Article

On Demand Release of Cerium from an Alginate/Cerium Complex for Corrosion Protection of AISI1020 and AA2024 Substrates

Bruno C. da Silva, [a,b] Alexandre C. Bastos, [c] João Tedim, [c] Mário G. S. Ferreira, [c]
Cláudia E. B. Marino [b] and Izabel C. Riegel-Vidotti [*,a]

[a]Grupo de Pesquisa em Macromoléculas e Interfaces, Departamento de Química,
Universidade Federal do Paraná (UFPR), CP 19032, 81531-980 Curitiba-PR, Brazil

[b]Departamento de Engenharia Mecânica, Universidade Federal do Paraná (UFPR),
81531-980 Curitiba-PR, Brazil

[c]Departamento de Engenharia de Materiais e Cerâmica, CICECO,
Universidade de Aveiro, 3810-193 Aveiro, Portugal

Alginate (ALG) is a natural polymer used in a wide range of applications. Cerium is a sustainable corrosion inhibitor for many metal substrates. In this study, ALG/Ce^{3+} hydrogel microparticles are presented as an innovative cerium(III) reservoir system for the smart release of cerium ions. The active corrosion inhibition capacity of the ALG/Ce^{3+} complex was investigated. Tests using ALG/Ce^{3+} macrogels (beads) and electrochemical experiments showed that, in saline media, ALG/Ce^{3+} hydrogel was able to release Ce^{3+}, which was subsequently exchanged with Al^{3+}, Fe^{2+} and Fe^{3+} and, thus slowing the corrosion process of AA2024 (aluminum alloy) and AISI1020 (carbon steel) substrates, respectively. It is suggested that the presence of metal ions originated from the corrosion process triggers the cerium release. The corrosion protection of ALG/Ce^{3+} of the aluminum alloy was confirmed by polarization curves, electrochemical impedance spectroscopy (EIS) and scanning vibrating electrode technique (SVET) and the protection of the carbon steel was demonstrated by EIS experiments. To the best of our knowledge, this is the first time that an alginate-based complex has been reported as an ion exchange corrosion-inhibiting system for metal substrates.

Keywords: EIS, corrosion resistance, ion exchanger, carbon steel, aluminum alloy, hydrogel

Introduction

Corrosion is a major problem worldwide, since about 3-4% of the gross domestic product (GDP) of each country is spent on direct or indirect costs related to corrosion.[1] In this context, finding solutions to reduce or avoid corrosive processes is of utmost economic interest. Organic,[2] metallic and inorganic compounds[3] have been used to protect various metal surfaces.[4] Organic coatings such as paints and resins are widely employed to prevent corrosion. Polymeric coatings are able to form films, protecting the metal against corrosion by physically blocking the contact of corrosive agents with the surface. One disadvantage is that the physical barrier's efficiency depends on the adhesive forces between the film and the interface, as

well as the porosity and mechanical properties of the film. Defects such as microcracking and delamination, which tend to form when the coated structures are exposed to weathering conditions during the structure service life, are difficult to identify and remediate readily.[5] Organic coatings loaded with corrosion inhibitors (either organic molecules or inorganic moieties that are able to adhere on the metal surface), have been applied to increase corrosion protection. In this way, when the coating barrier effect (passive protection) fails, the corrosion inhibitors act directly on the metal surface reducing the corrosion rate (active protection). Nevertheless, there are several challenges associated with the direct insertion of corrosion inhibitors in coating formulations, including the occurrence of undesirable reactions between the components of the coating and the corrosion inhibitors and spontaneous leaching.[4,6] Corrosion inhibitors can be cathodic, anodic or by adsorption. Rare earth metal

compounds are of great interest for cathodic inhibition. Their salts act by blocking the cathodic areas because of the precipitation of a film containing the rare earth oxide/hydroxide.[7] Rare earth hydroxides are in general soluble in acidic media and insoluble in alkaline media, have low toxicity and are economically advantageous.[8,9] Among them, cerium nitrate is a low-toxicity cathodic inhibitor.[10] In the presence of air and in aqueous media, the main cathodic reaction is the reduction of oxygen followed by the precipitation of $Ce(OH)_3$ on cathodic areas,[11] since the critical precipitation pH of cerium(III) hydroxide is 8.57 (100 ppm).[7,11] Equations 1 and 2 illustrate the process:

$$2H_2O_{(l)} + O_{2(g)} + 4e^- \rightarrow 4OH^-_{(aq)} \qquad (1)$$
$$Ce^{3+}_{(aq)} + 3OH^-_{(aq)} \rightarrow Ce(OH)_{3(s)} \qquad (2)$$
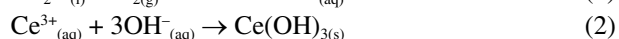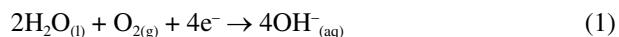
Recently, new approaches that offer active protection against corrosion, while attempting to overcome the aforementioned detrimental effects associated with direct addition of corrosion inhibitors to coatings, have been proposed. These include the development of materials with the ability to store and release corrosion inhibitors on demand.[12-15] Accordingly, the active material is isolated from the external environment, in a micro or nanocontainer, or even homogeneously distributed in the container, where it is released on demand. The release may be triggered by different stimuli, such as the presence of certain ions, changes in pH or temperature, among others.[12-14,16,17] Coatings loaded with micro/nanocontainers with immobilized corrosion inhibitors are generally termed as smart coatings, due to their ability of supplying corrosion inhibitors in a controllable way.[14,18] In one relevant study, clay minerals containing cerium were tested in a coating based on silane to protect galvanized steel, and presented corrosion resistance approximately twice that of the reference coating.[19]

Polymers obtained from natural sources have been used for a long time to prepare systems for sustained release, mainly for pharmaceutical and biomedical applications.[20-22] Alginate (ALG) is a naturally occurring polymer typically extracted from brown algae and has been widely used in many fields due to its biocompatibility, low toxicity, relatively low cost and moderate gelling properties by the addition of polyvalent cations such as Ca^{2+} and Fe^{3+}. Chemically, alginate is a linear copolymer composed of blocks of $(1\rightarrow4)$-linked β-D-mannuronic (M) and α-L-guluronic (G) acids. The monomers can be arranged in sequences of the same monosaccharide (G-blocks or M-blocks) or can be alternated (random G/M blocks).[22] Alginates produce gels because of the exchange of sodium ions (from sodium alginate) with Ca^{2+} (and other divalent cations) and higher valence cations. This process is referred to as ionotropic gelation.[23,24] Many studies have been performed to understand the nature of the interactions between cations (mono, di and trivalent) and the monomeric units G and M of alginate. Mineva and co-workers[24] used a quantum-mechanical density functional theory (DFT)-based method to study the complexation of various divalent cations with M and G disaccharides arranged in a large number of possible combinations, with and without water in the inner coordination shells. They also studied, by the same method, the complexation of alginate with M units to many trivalent ions.[23] In the first investigation, they found that the complexation of disaccharides with transition metal divalent ions formed strong coordination-covalent bonds, whereas the complexation with alkaline earth cations formed ionic bonds. In the case of trivalent ion complexation, the authors reported that all hydrated alginate structures formed bonds energetically more favored with $M^{3+}---(COO^-)$ than with $M^{3+}---O(OH)$. They also found a strong covalent contribution to the coordination of trivalent ions, similar to what was observed in the case of divalent transition metal cations. More recently, Fang and co-workers[25] reviewed in more details the gelation mechanism of alginate. They proposed that trivalent ions can bind to carboxyl groups of uronates with no selection towards G, M or GM blocks whereas divalent ions show different selection.

The present work was aimed at developing responsive hydrogel particles for anticorrosion applications. The corrosion inhibitor Ce^{3+} was immobilized in an alginate matrix and released in the presence of chemical species associated with the onset of the corrosion of the metallic substrate (e.g., Fe^{2+}, Fe^{3+} and Al^{3+}). The results demonstrated that alginate microgels have applications in smart coatings for corrosion protection of different metals, in saline media. Polarization curves, electrochemical impedance spectroscopy (EIS) and scanning vibrating electrode technique (SVET) were used to study ALG/Ce^{3+} as an anticorrosive material for aluminum alloy (AA2024, commonly used in the aircraft industry). The protection of ALG/Ce^{3+} of the carbon steel (AISI1020, commonly used in the petrochemical industry) was evaluated by EIS. Both substrates have high commercial importance. To the best of our knowledge, this is the first time that a polysaccharide complex has been proposed as an effective anticorrosive material. The hydrogel presented here meets the main principles of green chemistry, contributing to reduce the environmental and health impacts associated with the use of synthetic materials for corrosion protection.

Experimental

Materials

Sodium alginate and Ce(NO$_3$)$_3$ (Sigma-Aldrich, Darmstadt, Germany), NaCl, CaCl$_2$, Al$_2$(SO$_4$)$_3$, FeCl$_3$, FeCl$_2$, CuSO$_4$, ZnCl$_2$, (Synth, Diadema, SP, Brazil) and solvents ethanol, acetone and isopropanol (Tedia Brazil, Rio de Janeiro, Brazil) were of analytical grade used without further purification. The metallic substrates (1 cm × 1 cm × 1 mm), used in the electrochemical experiments, were AA2024 aluminum alloy and AISI1020 carbon steel (Barranco Ferro e Aço, Curitiba, PR, Brazil).

Ionotropic gelation of alginate

Alginate hydrogel particles were prepared by ionotropic gelation, following two different protocols. Alginate macrogels (beads of around 1 mm) were prepared by the dipping technique. First, a 2 wt.% ALG aqueous solution was prepared in distilled water. After stirring at room temperature, 5 mL of the solution was added dropwise to 20 mL of the gelling solution (0.1 mol L^{-1}) at 200 µL min^{-1}. The gelling solution was FeCl$_2$, FeCl$_3$, Al$_2$(SO$_4$)$_3$, Ce(NO$_3$)$_3$, CaCl$_2$, CuSO$_4$ or ZnCl$_2$. After the complete addition of alginate, the beads were left in the gelling solutions for 30 min longer, under mild stirring, washed five times with distilled water and dried for 12 h at 45 °C. Around 0.1 g of dried beads was added to 20 mL of NaCl, FeCl$_3$, Al(NO$_3$)$_3$, CuSO$_4$ or ZnCl$_2$ (50 mmol L^{-1}) and left for 24 h. After, the beads were removed from the test solution and dried on paper towels for further analysis. The ion exchange capacity of the macrogels was assessed by their visual inspection. Iron, aluminum, copper and zinc salt solutions were chosen because their cations are common in anti-corrosion products to protect metal and metal alloys of commercial interest. Calcium ions were chosen for comparison because there are commonly used to prepare alginate.

Alginate microgels (particles of around 10 µm) were prepared by a diffusion-controlled method and used in the electrochemical tests. First, a 5 wt.% ALG aqueous solution was prepared in distilled water. Then Ce(NO$_3$)$_3$ (10 mmol L^{-1}) was added dropwise, under vigorous stirring (15,000 rpm) to the alginate solution until 3.0 mmol Ce^{3+} *per* gram of alginate was reached. A more concentrated cerium solution (100 mmol L^{-1}) was added to the previous mixture until 10 mmol Ce^{3+} *per* gram of alginate, at the same stirring rate. The system was left under stirring for an additional 30 min. Then, the microparticles were obtained by vacuum filtering with a Buchner funnel and washed with isopropanol until completely dried. The amount of water and the amount of cerium in wt.% dry basis in the microgel particles were determined using a Setaram Labsys TGD SC 16 thermogravimetric (TG) analyzer (SETARAM Instrumentation, France) in an oxygen atmosphere at a heating rate of 10 °C min^{-1} from room temperature to 900 °C.

Preparation of metallic substrates for electrochemical tests

The substrates (dimensions: 1 × 1 × 1 cm) of AA2024 aluminum alloy and AISI1020 carbon steel were prepared with external electrical contacts of copper wire inserted in a Teflon mold and then embedded in an epoxy resin (araldite). The carbon steel working electrode surfaces were abraded using different grit sizes of abrasive papers (360, 600, 800), washed with distilled water, alcohol and acetone and then dried using compressed air. A working area of 1 cm^2 was left in contact with 10 mL of the test solution.

Electrochemical impedance spectroscopy (EIS)

The EIS technique was used to characterize bare AA2024 and bare AISI1020 substrates in 50 mmol L^{-1} NaCl solution with ALG/Ce^{3+} microgel (5 g L^{-1} for AA2024 and 10 g L^{-1} for AISI1020 steel) and without the addition of microgels. The microgel concentration for AISI1020 was doubled since Fe-C alloys are notably more susceptible to corrosion. The measurements were carried out with a Gamry FAS2 Femtostat (Gamry Instruments, USA) coupled to a PCI4 controller at open circuit potential (OCP) with application of a 10 mV sinusoidal perturbation in the 10 kHz to 10 mHz frequency range, taking 7 points *per* decade. A conventional three-electrode cell was used: a saturated calomel reference electrode (Hg/Hg$_2$Cl$_2$/KCl), a platinum foil with an exposed area of about 30 mm^2 as the counter electrode, and AA2024 or AISI1020 sample as the working electrode. All the measurements were carried out in a Faraday cage in order to avoid electromagnetic interference, and the impedance plots were fitted using the Gamry Echem Analyst software version 5.61 (Gamry Instruments, USA). The EIS measurements were conducted to evaluate the performance of the protection against surface corrosion of the metal substrates with and without the presence the ALG/Ce^{3+} microgel in saline solution. Using the same device, we obtained the polarization curve for the AA2024 aluminum alloy, after immersion for 1 h in NaCl 50 mmol L^{-1}, with and without addition of ALG/Ce^{3+} (5 g L^{-1}), in the potential range from −1.4 to −0.1 V (*vs.* saturated calomel electrode (SCE)) with scanning speed of 0.01 mV s^{-1}. The potentiodynamic polarization technique was used to investigate the kinetics of the processes that occur

in the metal substrate at potentials other than the open-circuit potential in the solution containing chloride ions.

The SVET (scanning vibrating electrode technique) measurements were carried out with an Applicable Electronics system (Applicable Electronics Inc., USA) with platinum micro-electrode (10 μm), vibration frequencies on the x and z axes of 115 and 69 Hz, respectively, and vibration amplitude of 10 μm, at a distance of 100 μm from the surface. The maps were composed of 35×35 points with intervals of 0.2 s between each measurement, in a solution of NaCl 50 mmol L^{-1}. The cathodic regions are represented in blue and the anodic regions in red. The SVET technique allows obtaining a map of the cathodic and anodic current densities occurring on the metal surface.

Results and Discussion

Cation exchange capacity of ALG/Ce^{3+} beads

As proof-of-concept, ALG/M^{n+} beads (macrogels) were prepared and their behavior in contact with different saline solutions was macroscopically evaluated with the intention of assessing the ion exchange capacity of ALG/Ce^{3+} with other cations. To investigate the application for corrosion inhibition, besides Ce^{3+} (lanthanide), the following di and trivalent cations were also selected as crosslinking agents: Ca^{2+} (alkaline earth), Cu^{2+}, Zn^{2+} and Fe^{3+} (transition metals), and Al^{3+} (metal).

Alginate beads were obtained crosslinked with all chosen cations. The corresponding hydrated beads

(as-prepared) can be seen in Figure 1, first column. The smallest beads (2.0 ± 0.1 mm) were obtained when Cu^{2+} was used as crosslinker, whereas the largest ones (2.9 ± 0.2 mm) were obtained with Fe^{3+}. In addition, the Al^{3+} beads had an elongated shape (2.8 ± 0.1 mm × 2.0 ± 0.1 mm), which may be related to the slow reticulation rate of alginate by Al^{3+} ions. As the alginate droplets fall into the crosslinking solution (see Experimental section), the low reaction rate associated with the stirring speed causes the droplet to deform into an elongated shape that remains throughout the entire process. Beads produced using the other cations as crosslinkers were spherical (around 2.0 mm) because the fast-crosslinking rate causes the formation of a rigid membrane around the droplet in a very short time, preserving its shape despite the shear stress from stirring. The water content, determined by a gravimetric method, was approximately 95 wt.% for all hydrogels.

To evaluate the behavior of the ALG/M^{n+} complexes, beads were dried and rehydrated, as described in the Experimental section. The type of cations and the swelling solution pH were varied. All beads maintained their shape after drying (Figure 1, second column). When immersed in solutions with pH 2 or pH 10 (Figure 1, third and fourth columns), alginate beads crosslinked with Ca^{2+}, Fe^{3+}, Ce^{3+} and Cu^{2+} did not rehydrate (i.e., did not swell). Conversely, alginate beads crosslinked with Zn^{2+} and Al^{3+} swelled at pH 2 and pH 10, in a higher amount in the latter case (at pH 10). Also, the highest swelling degree was observed for ALG/Al^{3+} after immersion in the solution with pH 10. It is possible to induce alginate gelation by lowering pH
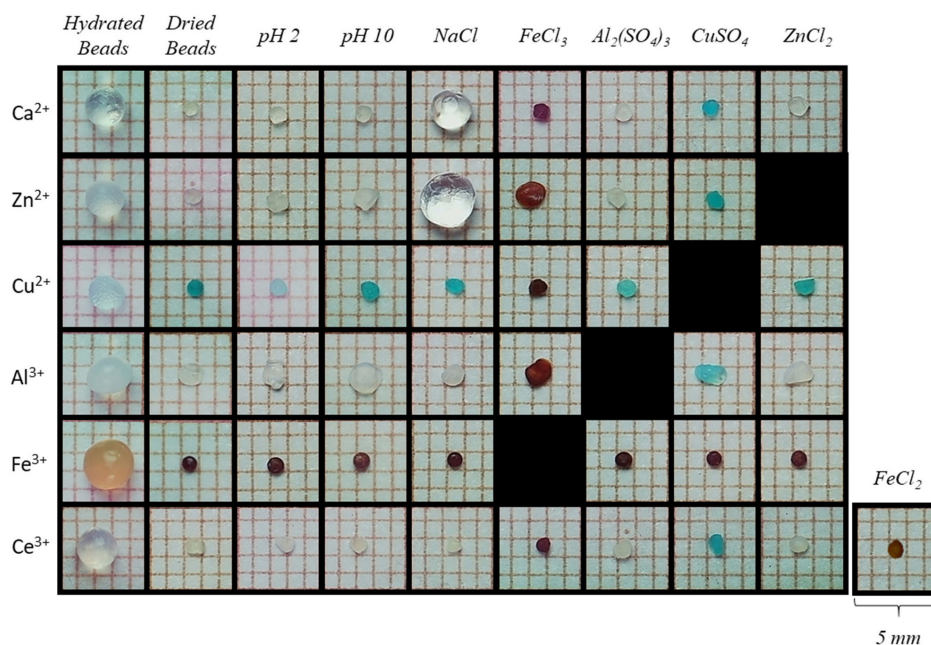

Figure 1. Visual analysis of the behavior of ALG/M^{n+} beads, using Ca^{2+}, Zn^{2+}, Cu^{2+}, Al^{3+}, Fe^{3+} and Ce^{3+} as crosslinking agents: shape, rehydration and exchange capacity in the indicated saline solutions, at 50 mmol L^{-1}.

below the pK_a values, i.e., 3.4 and 3.6 for M and G units, due to intra and interchain interactions.[26] In this case, the cations will be mainly imprisoned within the polymer matrix, being the release driven by diffusion and not by ion-exchange mechanisms. At pH higher than the M and G pK_a values, polymer-cation interactions will be favored. When the beads were immersed in 50 mmol L^{-1} NaCl, there was high degree of swelling of ALG/Ca^{2+} and ALG/Zn^{2+}, while the other complexes were not affected (compare the second and the fifth columns).

The ion exchange capacity of all dried beads was evaluated by immersion in 50 mmol L^{-1} of $FeCl_3$, $Al_2(SO_4)_3$, $CuSO_4$ or $ZnCl_2$ aqueous solution (Figure 1, from 6th to 9th columns). When immersed in $FeCl_3$, all beads' color changed, evidencing the insertion of Fe^{3+} into the alginate matrix. Of particular note was the swelling of ALG/Zn^{2+} and ALG/Al^{3+} after immersion in $FeCl_3$. In contrast, the ALG/Fe^{3+} beads did not interact with any of the other cation solution, demonstrating the stability of this complex. Except for ALG/Fe^{3+}, all beads turned blue when immersed in $CuSO_4$ and displayed a small degree of swelling when immersed in $Al_2(SO_4)_3$, suggesting a certain degree of exchange of Ca^{2+}, Zn^{2+}, Ce^{3+} and Al^{3+} for Cu^{2+} and of Ca^{2+}, Zn^{2+}, Ce^{3+} and Cu^{2+} for Al^{3+}. Dry ALG/Ce^{3+} beads, when immersed in $ZnCl_2$ solution, did not change their shape, and when immersed in Fe^{2+} solution, the result was similar to that with Fe^{3+}, i.e., a pronounced color change. According to the observations, the ALG/M^{n+} affinity increases in the order: $Zn^{2+} < Ca^{2+} < Ce^{3+} < Al^{3+} \leq Cu^{2+} < Fe^{3+}$, which agrees with what has been reported in the literature.[24,27-30]

The interactions between alginate and many cations were studied by Mineva and co-workers.[23,24] According to them, Ca^{2+} as well as all alkaline earth metals interacted with uronates by ionic bonding, evidenced by the distance between the atoms participating in the bond, with no orbital overlap. Transition metals, on the other hand, formed strong coordination-covalent bonds with the disaccharide (MG), confirmed by the shorter interatomic distance, with orbital overlap. These facts explain the behavior of ALG/Ca^{2+} beads in the presence of NaCl (see Figure 1). The ionic bonding character seems to facilitate the exchange of Ca^{2+} with Na^+, due to the larger bonding distance and the small ionic radius difference between Na^+ and Ca^{2+}, 102 and 100 pm, respectively. The exchange of Ca^{2+} with Na^+ leads to the physical deconstruction of the gel, loosening its network and allowing the entrance of water, resulting in the increase in the gel's hydration degree. In saline media, the gel ALG/Zn^{2+} rehydrated more than the gel ALG/Ca^{2+}. Previous work demonstrated experimentally that alginate's affinity decreases in the following order: $Cu^{2+} > Ca^{2+} > Zn^{2+}$.[29,31] It was also reported that Zn^{2+}/uronate forms a

coordination-covalent bonds with relatively low energy when compared to other transition metals (Cu > Mn > Zn).[24] The electronic characteristics of Zn^{2+}, with all filled orbitals (closed-shell configuration), is responsible for the relatively weak interaction with alginate. The behavior observed for ALG/Fe^{3+} beads occurred because Fe^{3+} strongly interacts with the carboxylate groups in alginate,[32] forming strong coordination-covalent bonds. ALG/Fe^{3+} is a compact gel because Fe^{3+} has a small ionic radius (60 pm),[33] hindering the entrance of water molecules into the dried gel. The large initial volume of the gels (as formed) occurred due to the Fe^{3+}---O(OH) and Fe^{3+}---O(COO–) bond distances.[23] In the swelled gel, the first predominates, whereas in the dried gel, the second type of bond predominates, which is shorter and causes the shrinkage of the network. Among the trivalent ions, Ce^{3+} ions had the lowest affinity for alginate. The exchange of Ce^{3+} with Cu^{2+} is favored, possibly because of the lower ionic radius of Cu^{2+}.

The potential of the ALG/Ce^{3+} hydrogel for corrosion protection was qualitatively demonstrated since this system serves as a container for Ce^{3+} ions that, when in contact with Fe^{3+}, Al^{3+} and Cu^{2+}, are expected to be released to the environment, as supported by the literature and further evidenced by the EIS results. In addition, it is worth emphasizing that the preparation and application of this system is aligned with environmentally conscious processes, since both components have low toxicity and ALG is obtained from natural sources.

Assessment of ALG/Ce^{3+} as active corrosion inhibitor for AA2024 aluminum alloy

ALG/Ce^{3+} microgels were prepared to investigate the active corrosion inhibition against AA2024 corrosion. The cerium concentration in ALG/Ce^{3+} dry microgels, as determined by thermogravimetry, was 21 wt.%.

The result of the polarization curve test (Figure 2) obtained for the aluminum alloy showed that the reactions occurred with different kinetics. It is observed that the aluminum alloy starts to present a current density increase, near from the corrosion potential, reducing this density current increase around −0.5 V (*vs.* SCE), due to the formation of corrosion products. In the presence of ALG/Ce^{3+}, there is a lower current density involved, and with formation of corrosion products from −0.4 V (*vs.* SCE). The current density increase, from the open circuit potential (OCP), means that the AA2024 alloy peak potential is close to that value. Therefore, comparing the OCPs of the alloy in the absence and presence of the cerium ion, it can be said that in the absence of this ion, the beginning of the pits starts at a lower potential. The cathodic reaction is predominantly

controlled by diffusion due to the oxygen reduction reaction and also, it is possible to observe the water reduction reaction at potentials below approximately -1.0 V (*vs*. SCE). The localized corrosive process is limited by the cathodic reaction, which is usually slower than the anodic reaction.[34] These results indicate that the free Ce^{3+} ions react with the hydroxyls resulting from the cathodic reaction (equation 1) forming $Ce(OH)_3$ (equation 2), that is a hydroxide with low solubility that precipitates[35,36] with the local alkalinization of the medium and forms a protective layer on the cathodic region of the active metal. The deposition of a compact and adherent film on the metal restricts the species diffusion, increasing the resistance to pitting corrosion on the surface of the AA2024 alloy. Furthermore, independently of the concentration, a cathodic inhibitor always has a positive effect on protection, so it stands out in relation to the use of an anodic inhibitor[4] that, if not used in sufficient concentration, can even increase the corrosion rate.
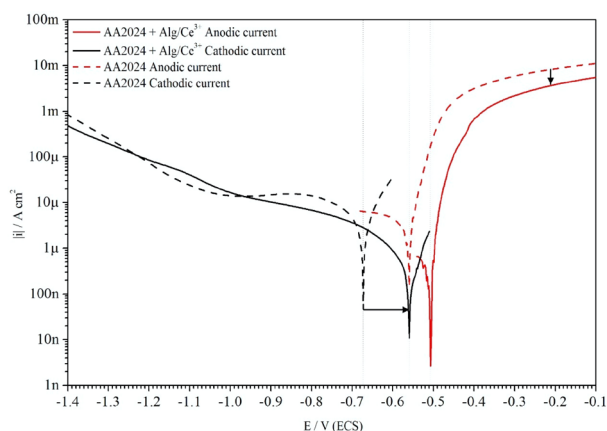

Figure 2. Polarization curves of AA2024 with and without the presence of ALG/Ce^{3+} (5 g L^{-1}), after 1 h in NaCl 50 mmol L^{-1}.

Figure 3 displays the electrochemical impedance spectra (Bode plots) of AA2024 aluminum alloy, in 50 mmol L^{-1} NaCl, without (Figure 3a) and with (Figure 3b) the addition of ALG/Ce^{3+} (5 g L^{-1}) after 2 and 12 h of immersion. Regardless of the frequency, the impedance was higher in the presence of microgel, having an impedance at low frequency (0.01 Hz) > 100 kΩ cm^2 while in the absence this value was only > 10 kΩ cm^2. These values are directly correlated to the measure of corrosion resistance.[37] The Bode phase diagram of the sample without added microgel has a time constant in the high frequency region (ca. 1 kHz), related to the passivation layer on aluminum, consisting of Al_2O_3, and a time constant in the low region of frequency (ca. 8 Hz), related to the corrosion reaction of the substrate. When the aluminum oxide film formed on the surface of the AA2024 alloy is exposed to the medium containing chloride ions, attacks can occur at random points, causing localized

corrosion.[35,36] After exposure to the saline medium for 12 h, a third time constant was observed, possibly related to a diffusional control (phase angle ca. $-45°$) inside the pits.

The presence of the ALG/Ce^{3+} (Figure 3b) shifted the time constant related to the passive $Al_2O_3 + Ce(OH)_3$ layer to lower frequencies (ca. 500 Hz). The presence of a $Ce(OH)_3$ deposited on the top of the copper-containing inclusions of the AA2024 alloy (cathodic sites)[35,36] is responsible for the decrease of corrosion, inhibiting the cathodic reaction of oxygen reduction. The second time constant (ca. 1 Hz) can be associated with the electrochemical processes ongoing at the metal surface. A shoulder not well-defined occurring in the low frequency (ca. 30 mHz) could be related to the diffusion inside the pits although the time constant is not so evident. The impedance modulus (|Z|) at 0.01 Hz for AA2024, after 2 h in saline medium without microgels, was 12 kΩ cm^2, and increased to only 14 kΩ cm^2 after 12 h, while the system with ALG/Ce^{3+} microgels showed the higher |Z| value at the same frequency for 2 h (150 kΩ cm^2) with a subtle increase (157 kΩ cm^2) after 12 h of immersion in NaCl 50 mmol L^{-1}. These results are consistent to an active corrosion protection effect associated to the cerium ions released to the medium and the formation of a cerium hydroxide on the cathodic sites
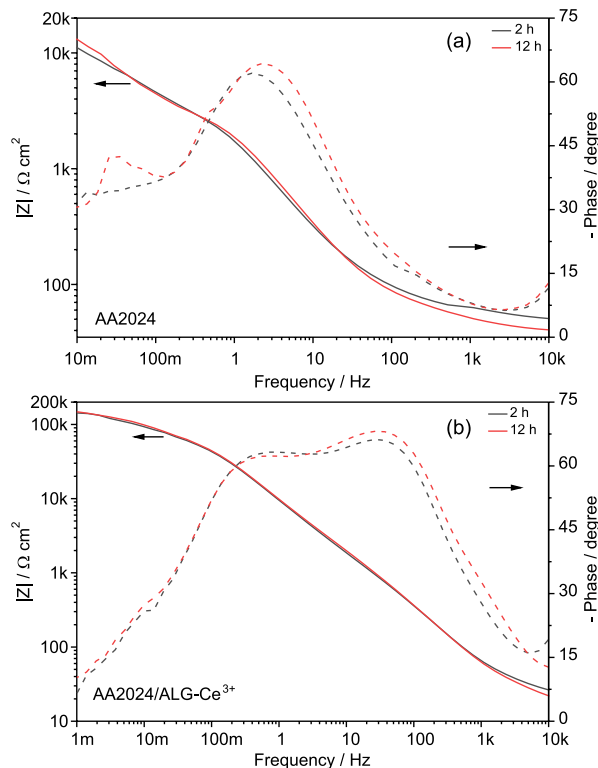

Figure 3. EIS Bode plots of AA2024 alloy in NaCl 50 mmol L^{-1}. (a) |Z| after 2 h (—) and 12 h (—) of immersion; and phase after 2 h (---) and 12 h (---) of immersion. (b) |Z| after 2 h (—) and 12 h (—) of immersion; and phase after 2 h (---) and 12 h (---) of immersion, both in the presence of ALG/Ce^{3+} microgel (5 g L^{-1}).

of the metal surface, increasing the corrosion resistance.[35,38] The corresponding Nyquist diagrams are shown in the Supplementary Information (SI) section (Figure S1).

The protection against pitting corrosion of the AA2024 alloy in the presence of the ALG/Ce^{3+} microgels was also proved by analyzing the metal surface by SVET (Figure 4), where the current density distributions were analyzed after immersion for 96 h in the solution containing chloride ions. Very few regions with positive current densities (red color), and thus regions with anodic activity indicating the exposure of the substrate to the localized corrosive action were observed in the presence of the intelligent ALG/Ce^{3+} system after that exposure time. The SVET map referring to the A2024 alloy (i.e., without the presence of the microgel), after exposure to the saline medium for 8 h, showed an intense pitting corrosion process (red area), evidenced by the high current density (460 µA cm^{-2}) and also the extensive blue area, indicating the equivalent cathodic activity (−30 to −100 µA cm^{-2}).

The presence of a barrier formed by cerium hydroxide was also proved by SVET (Figure 4), where after the addition of the ALG/Ce^{3+} microgels, pitting was totally absent after exposure to the saline medium for 12 h. After immersion for 4 days (96 h) in the medium containing chloride ions, there was only one low intensity pit, demonstrated by the magnitude of the current density, which was 15-fold lower compared to the localized corrosion process on the surface of the AA2024 alloy without microgel. The SVET results corroborated the results obtained by the electrochemical polarization and impedance techniques, demonstrating a fast and prolonged response of the ALG/Ce^{3+} microgel against pitting corrosion of the AA2024 alloy during the immersion period.

Assessment of ALG/Ce^{3+} as active corrosion inhibitor for AISI1020 carbon steel

The ALG/Ce^{3+} microgel particles were also tested with respect to their capacity to prevent corrosion of carbon steel (AISI1020). Figure 5 presents the Bode plots of bare carbon steel without microgels (Figure 5a) and in the presence of 10 g L^{-1} of ALG/Ce^{3+} (Figure 5b).

For the steel samples without addition of the microgel (Figure 5a), the EIS spectra showed that the surface was active and suffered a corrosion process in full progress, always presenting low impedance values (*y*-axis on the left) during the immersion time, i.e., around 2.5 kΩ cm^2 in the low frequency region. The Bode phase plots (*y*-axis on the right) shows mainly one relaxation process at 1 Hz, related to the corrosion reaction of iron[39,40] and a shoulder at 100 Hz indicating unstable iron corrosion products.[39,40]

In the corrosion process of AISI1020 carbon steel in saline media, the Fe^{2+} ions formed (Fe$_{(s)}$ → Fe$^{2+}_{(aq)}$ + 2e$^-$), in the presence of corrosive species as oxygen, water molecules and chloride ions, generate unstable iron oxides and hydroxides.[4,41]

In the presence of ALG/Ce^{3+} (Figure 5b), in the first 12 h of immersion, a relaxation process at medium frequency (60 Hz), corresponding to the corrosion of AISI1020. The
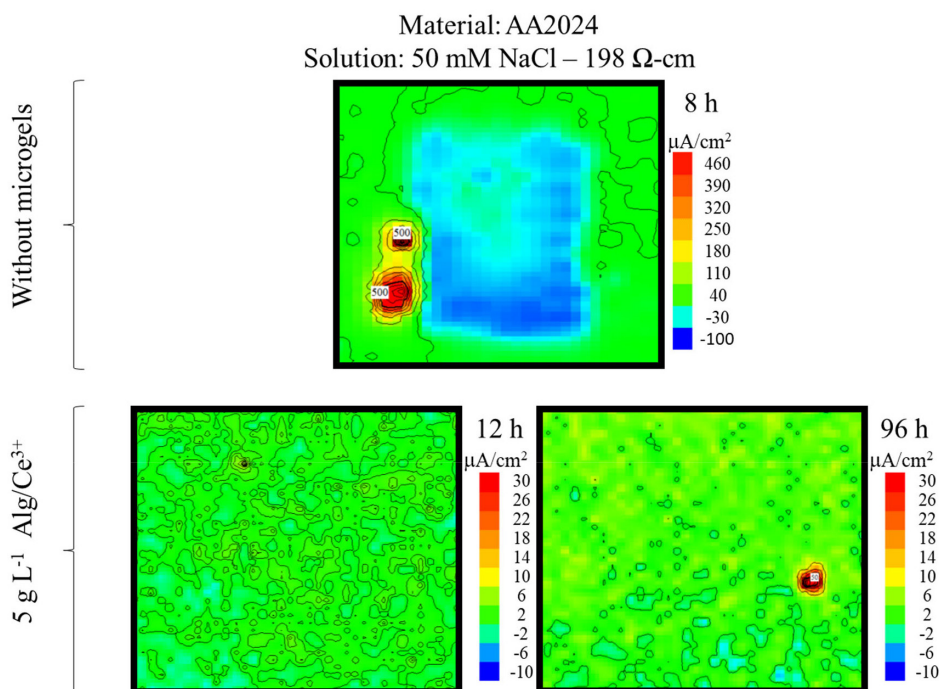

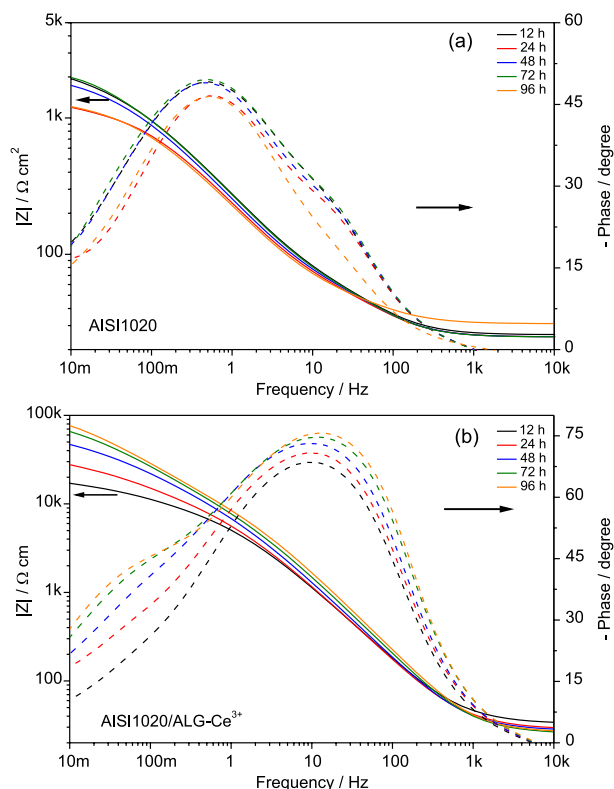**Figure 4.** SVET map of AA2024, in NaCl 50 mmol L^{-1} (a) without microgels; and (b) and (c) in presence of ALG/Ce^{3+} (5 g L^{-1}).

Figure 5. EIS Bode plots of carbon steel (AISI 1020) in NaCl 50 mmol L^{-1} (a) without microgels and (b) in the presence of 10 g L^{-1} ALG/Ce^{3+}.

presence of iron ions released by the occurrence of the corrosive process triggers the release of Ce^{3+} ions from the alginate particles. With increased exposure time, the |Z| shifts to higher values, reaching 100 kΩ cm^2 at low frequencies, possibly as a consequence of formation of corrosion products and deposition of a cerium protective layer.[40,42] The time constant at lower frequencies (150 mHz) for 72 and 96 h can be related with this latter process and

thus diffusion control. The protective system exists in a dynamic equilibrium between the protective layer and the medium, where the deposition and dissolution processes depend on the concentration of reagents and environmental conditions.[43,44] Thus, as long as the microgels can provide sufficient cerium to form and sustain the protective cerium layer, the metal surface will be protected. The corresponding Nyquist diagrams are shown in the SI section (Figure S2).

Comparative analysis ALG/Ce^{3+} action for the corrosion protection on AA2024 and AISI1020 surfaces

Unlike observed for the AA2024 aluminum alloy, the corrosion products of iron form a unstable layer that does not function as a barrier to reactive species, besides being subject to large volumetric variation during the change from the oxidative state of the products formed, leading to rupture of the surface film.[39,40] When cerium ions are free in the medium, they react with the OH$^-$ ions resulting from the cathodic reaction, thus forming cerium hydroxide, contributing to the corrosion protection.[35,38,43,44]

The EIS tests indicated better protection of the AA2024 aluminum alloy, even when employing twice the concentration of the ALG/Ce^{3+} smart system for protection of AISI1020 carbon steel. At an immersion time of 12 h, the impedance modulus was around 150 kΩ cm^2 (Figure 3) for the AA2024 alloy and 20 kΩ cm^2 (Figure 5) for the carbon steel.

All these results and mechanisms discussed corroborate the release of Ce^{3+} in the medium with deposition of cerium hydroxide that contributed to the corrosion resistance, as schematically illustrated in Figure 6 (Figure 6a-AA2024 and Figure 6b-AISI1020).
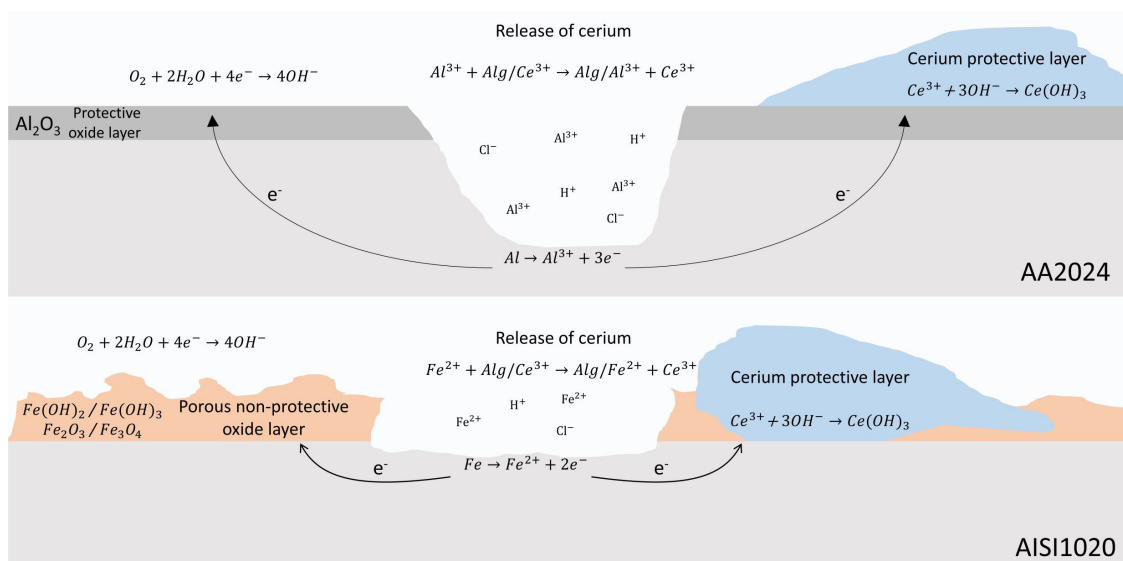

Figure 6. Schematic representation of the action mechanisms of ALG/Ce^{3+} beads on (a) AA2024 and (b) AISI1020 surfaces.

Considering that the ALG/Ce^{3+} beads were not affected by the saline medium, but had their properties changed when immersed in the Al^{3+}, Fe^{2+} and Fe^{3+} solutions (Figure 1), it is possible to infer that the results observed in the electrochemical experiments are a consequence of ionic exchange between the Ce^{3+} ions and Al^{3+}, Fe^{2+} and Fe^{3+} ions resulting from the corrosion of AA2024 and AISI1020.

The oxide layer formed by iron oxides is porous and poorly attached to the surface due to the high-volume difference among the iron corrosion products, leading to poor protection of these oxide layers. When the ALG/Ce^{3+} interacts with Fe$^{2+/3+}$ ions and removes them from the medium, the formation of the porous oxide layer is hindered, and the deposition of a cerium-containing layer is favored instead, which is more compact and provides better protection.

All the results showed that alginate has strong potential for use as an ion exchanger, which can improve the storage of cations with corrosion inhibiting activity. This study reports for the first time the application of alginate for the purpose of carrying and releasing cerium to protect against corrosion.

Conclusions

Sodium alginate was able to complex with cerium ions, forming a hydrogel that acted as a reservoir of anticorrosive Ce^{3+} ions. When in the presence of Fe^{3+}, Fe^{2+}, Al^{3+} and Cu^{2+} (for example, from a corrosive process), ALG/Ce^{3+} undergoes ion-exchange processes, thus free Ce^{3+} ions are released to the medium, without the presence of any counter-ions. Visual observation, polarization, EIS and SVET tests demonstrated the performance of the released cerium ions in the corrosion protection of AA2024 aluminum alloy, in saline solution. EIS also revealed the same effect in the protection of AISI1020 carbon steel. The protection promoted by cerium(III) occurs independently of the hydrogel integrity and leads to the formation of a passive Ce(OH)$_3$ layer on the substrate. The use of alginate/Ce^{3+} complex as an effective, sustainable and long-lasting anticorrosive material is innovative and demonstrated here for the first time. Finally, the smart system proposed here has low environmental impact due to the substances employed, a natural polymer (alginate) and a corrosion inhibitor with low toxicity (cerium) and is also innovative regarding the on-demand release of the inhibitor. These factors can increase the efficiency and time of protection against corrosion.

Supplementary Information

Supplementary information (Nyquist diagrams) is available free of charge at http://jbcs.sbq.org.br as PDF file.

Acknowledgments

Author Contributions

B. C. Silva was responsible for investigation, conceptualization, methodology, validation, visualization, writing original draft; A. C. Bastos for investigation, methodology, writing original draft; J. Tedim for supervision, methodology, writing original draft; M. G. S. Ferreira for supervision, methodology, funding acquisition, writing original draft; C. E. B. Marino for supervision, funding acquisition, methodology, conceptualization, writing original draft; I. C. Riegel-Vidotti for supervision, funding acquisition, methodology, conceptualization, writing original draft.

References

1. Varney, J.; Thompson, N.; Moghissi, O.; Gould, M.; Payer, J.; *International Measures of Prevention, Application, and Economics of Corrosion Technologies Study*; NACE International: Dublin, Ohio and APQC, Houston, Texas, USA, 2016. [Link] accessed in March 2022

2. Grundmeier, G.; Schmidt, W.; Stratmann, M.; *Electrochim. Acta* **2000**, *45*, 2515. [Crossref]

3. Maaß, P. In *Handbook of Hot-Dip Galvanization*; Wiley-VCH Verlag GmbH & Co. KGaA: Weinheim, Germany, 2011, ch. 1. [Crossref]

4. Revie, R. W.; Uhlig, H. H.; *Corrosion and Corrosion Control*, 4th ed.; John Wiley & Sons, Inc.: Hoboken, USA, 2008. [Crossref]

5. Hihara, L. H. In *Intelligent Coatings for Corrosion Control*, 1st ed.; Tiwari, A.; Hihara, L. H.; Rawlins, J., eds.; Elsevier: Waltham, USA, 2015, ch. 1. [Crossref]

6. Makhlouf, A. S. H. In *Handbook of Smart Coatings for Materials Protection*; Makhlouf, A. S. H. ed.; Elsevier: Waltham, USA, 2014, ch. 3. [Crossref]

7. de Damborenea, J.; Conde, A.; Arenas, M. A. In *Rare Earth-Based Corrosion Inhibitors*; Forsyth, M.; Hinton, B., eds.; Elsevier: Waltham, USA, 2014, ch. 3. [Crossref]

8. Mishra, A. K.; Balasubramaniam, R.; Tiwari, S.; *Anti-Corros. Methods Mater.* **2007**, *54*, 37. [Crossref]

9. Claux, B.; Serp, J.; Fouletier, J.; *Electrochim. Acta* **2011**, *56*, 2771. [Crossref]

10. Bennett, G. J.; *Hazard. Mater.* **2005**, *119*, 258. [Crossref]

11. Behrsing, T.; Deacon, G. B.; Junk, P. C. In *Rare Earth-Based Corrosion Inhibitors*; Forsyth, M.; Hinton, B., eds.; Elsevier: Waltham, USA, 2014, ch. 1. [Crossref]

12. Tedim, J.; Kuznetsova, A.; Salak, A. N.; Montemor, F.; Snihirova, D.; Pilz, M.; Zheludkevich, M. L.; Ferreira, M. G. S.; *Corros. Sci.* **2012**, *55*, 1. [Crossref]

13. Dias, S. A. S.; Lamaka, S. V.; Nogueira, C. A.; Diamantino, T. C.; Ferreira, M. G. S.; *Corros. Sci.* **2012**, *62*, 153. [Crossref]

14. Zheludkevich, M. L.; Tedim, J.; Ferreira, M. G. S.; *Electrochim. Acta* **2012**, *82*, 314. [Crossref]

15. Javidparvar, A. A.; Naderi, R.; Ramezanzadeh, B.; *J. Hazard. Mater.* **2020**, *389*, 122135. [Crossref]

16. da Cunha, A. B. M.; Leal, D. A.; Santos, L. R. L.; Riegel-Vidotti, I. C.; Marino, C. E. B.; *Surf. Coat. Technol.* **2020**, *402*, 126338. [Crossref]

17. Leal, D. A.; Riegel-Vidotti, I. C.; Ferreira, M. G. S.; Marino, C. E. B.; *Corros. Sci.* **2018**, *130*, 56. [Crossref]

18. Shchukin, D. G.; Möhwald, H.; *Small* **2007**, *3*, 926. [Crossref]

19. Motte, C.; Poelman, M.; Roobroeck, A.; Fedel, M.; Deflorian, F.; Olivier, M.-G.; *Prog. Org. Coat.* **2012**, *74*, 326. [Crossref]

20. Li, P.; Dai, Y.-N.; Zhang, J.-P.; Wang, A.-Q.; Wei, Q.; *Int. J. Biomed. Sci.* **2008**, *4*, 221. [Link]

21. Kaygusuz, H.; Torlak, E.; Akın-Evingür, G.; Özen, İ.; von Klitzing, R.; Erim, F. B.; *Int. J. Biol. Macromol.* **2017**, *105*, 1161. [Crossref]

22. Lee, K. Y.; Mooney, D. J.; *Prog. Polym. Sci.* **2012**, *37*, 106. [Crossref]

23. Menakbi, C.; Quignard, F.; Mineva, T.; *J. Phys. Chem. B* **2016**, *120*, 3615. [Crossref]

24. Agulhon, P.; Markova, V.; Robitzer, M.; Quignard, F.; Mineva, T.; *Biomacromolecules* **2012**, *13*, 1899. [Crossref]

25. Hu, C.; Lu, W.; Mata, A.; Nishinari, K.; Fang, Y.; *Int. J. Biol. Macromol.* **2021**, *177*, 578. [Crossref]

26. Gurikov, P.; Smirnova, I.; *Gels* **2018**, *4*, 14. [Crossref]

27. Haug, A.; Smidsrød, O.; Larsen, B.; Gronowitz, S.; Hoffman, R. A.; Westerdahl, A.; *Acta Chem. Scand.* **1965**, *19*, 341. [Crossref]

28. Jodra, Y.; Mijangos, F.; *Water Sci. Technol.* **2001**, *43*, 237. [Crossref]

29. Ionita, G.; Ariciu, A. M.; Smith, D. K.; Chechik, V.; *Soft Matter* **2015**, *11*, 8968. [Crossref]

30. Kaygusuz, H.; Erim, F. B.; Pekcan, Ö.; Akın Evingür, G.; *J. Fluoresc.* **2014**, *24*, 161. [Crossref]

31. Rezaii, N.; Khodagholi, F.; *Protein J.* **2009**, *28*, 124. [Crossref]

32. Bruchet, M.; Melman, A.; *Carbohydr. Polym.* **2015**, *131*, 57. [Crossref]

33. Schaeffer Jr., C. D.; Strausser, C. A.; Thomsen, M. W.; Yoder, C. H.; *Data for General, Organic, and Physical Chemistry*; DocerArgentina, 1989. [Link] accessed in March 2022

34. Rendón, M. V.; Calderón, J. A.; Fernández, P.; *Quim. Nova* **2011**, *34*, 1163. [Crossref]

35. Yasakau, K. A.; Zheludkevich, M. L.; Lamaka, S. V.; Ferreira, M. G. S.; *J. Phys. Chem. B* **2006**, *110*, 5515. [Crossref]

36. Szklarska-Smialowska, Z.; *Corros. Sci.* **1999**, *41*, 1743. [Crossref]

37. Taheri, P.; Milošev, I.; Meeusen, M.; Kapun, B.; White, P.; Kokalj, A.; Mol, A.; *npj Mater. Degrad.* **2020**, *4*, 12. [Crossref]

38. Yasakau, K. A.; Tedim, J.; Montemor, M. F.; Salak, A. N.; Zheludkevich, M. L.; Ferreira, M. G. S.; *J. Phys. Chem. C* **2013**, *117*, 5811. [Crossref]

39. Calegari, F.; da Silva, B. C.; Tedim, J.; Ferreira, M. G. S.; Berton, M. A. C.; Marino, C. E. B.; *Prog. Org. Coat.* **2020**, *138*, 105329. [Crossref]

40. Ivušić, F.; Lahodny-Šarc, O.; Ćurković, H. O.; Alar, V.; *Corros. Sci.* **2015**, *98*, 88. [Crossref]

41. Sherif, E.-S. M.; *Int. J. Electrochem. Sci.* **2011**, *6*, 3077. [Link]

42. Dastgheib, A.; Mohammadzadeh Attar, M.; Zarebidaki, A.; *Met. Mater. Int.* **2020**, *26*, 1634. [Crossref]

43. Majdi, M. R.; Danaee, I.; Afghahi, S. S. S.; *Mater. Res.* **2017**, *20*, 445. [Crossref]

44. Stoyanova, E.; Stoychev, D. In *Corrosion Resistance*; Shih, H., ed.; IntechOpen: London, UK, 2012. [Link] accessed in March 2022